The Astrophysical Journal, 722:862–870, 2010 October 10 doi:10.1088/0004-637X/722/1/862

VERY HIGH ENERGY OBSERVATIONS OF GAMMA-RAY BURSTS WITH STACEE

A. Jarvis[1,8], R. A. Ong[1], D. A. Williams[2], T. Aune[2], J. Ball[1,9], J. E. Carson[1,10], C. E. Covault[3], D. D. Driscoll[3,11], P. Fortin[4,12], D. M. Gingrich[5,6], D. S. Hanna[7], J. Kildea[7,13], T. Lindner[7,14], R. Mukherjee[4], C. Mueller[7,15], K. Ragan[7], and J. Zweerink[1]

[1] Department of Physics and Astronomy, University of California, Los Angeles, CA 90095, USA
[2] Santa Cruz Institute for Particle Physics and Department of Physics, University of California, Santa Cruz, CA 95064, USA
[3] Department of Physics, Case Western Reserve University, Cleveland, OH 44106, USA
[4] Department of Physics, Columbia University, New York, NY 10027, USA
[5] Centre for Particle Physics, University of Alberta, Edmonton, AB T6G 2G7, Canada
[6] TRIUMF, Vancouver, BC V6T 2A3, Canada
[7] Physics Department, McGill University, Montreal, QC H3A 2T8, Canada
Received 2010 June 23; accepted 2010 August 17; published 2010 September 23

ABSTRACT

Gamma-ray bursts (GRBs) are the most powerful explosions known in the universe. Sensitive measurements of the high-energy spectra of GRBs can place important constraints on the burst environments and radiation processes. Until recently, there were no observations during the first few minutes of GRB afterglows in the energy range between 30 GeV and ∼1 TeV. With the launch of the *Swift* GRB Explorer in late 2004, GRB alerts and localizations within seconds of the bursts became available. The Solar Tower Atmospheric Cherenkov Effect Experiment (STACEE) was a ground-based, gamma-ray telescope with an energy threshold of ∼150 GeV for sources at zenith. At the time of *Swift*'s launch, STACEE was in a rare position to provide >150 GeV follow-up observations of GRBs as fast as three minutes after the burst alert. In addition, STACEE performed follow-up observations of several GRBs that were localized by the *HETE-2* and *INTEGRAL* satellites. Between 2002 June and 2007 July, STACEE made follow-up observations of 23 GRBs. Upper limits are placed on the high-energy gamma-ray fluxes from 21 of these bursts.

Key words: gamma-ray burst: general – gamma-ray burst: individual (GRB 050509B, GRB 050607) – gamma rays: general

Online-only material: color figures

1. INTRODUCTION

The first gamma-ray burst (GRB) detections were reported in 1973 (Klebesadel et al. 1973). Two decades later, more than 100 GRB models had been proposed (e.g., Nemiroff 1994), and even whether the bursts were galactic or extragalactic events was still under debate. It was not until 1997, when the first afterglow detections were made at X-ray (Costa et al. 1997), optical (van Paradijs et al. 1997), and radio (Frail et al. 1997) wavelengths, that we began to dramatically narrow down the list of possible progenitors and emission processes. The observed properties of GRBs indicate that the ejecta from these powerful explosions are initially moving at highly relativistic speeds, making GRBs potential sources of very high energy (VHE; $E > 100$ GeV) gamma rays (Zhang & Mészáros 2001; Pe'er & Waxman 2005). However, there has not yet been an undisputed detection of a VHE GRB afterglow.

The spectra of GRB afterglows are typically well modeled as synchrotron emission from a population of relativistic electrons (Piran 1999). Some of the synchrotron photons are likely to be upscattered to very high energies before they can escape the plasma, a process known as synchrotron self-Compton (SSC) emission. The predicted strength of the SSC component of the GRB spectrum depends on the precise characteristics of the burst, such as the Lorentz factor of the ejecta, the strength of the magnetic field, and the density of the surrounding medium (Chiang & Dermer 1999; Sari & Piran 1997).

The Energetic Gamma-Ray Experiment Telescope (EGRET) on the Compton *Gamma-Ray Observatory* showed that burst spectra can extend to at least several GeV and saw no evidence of a cutoff (Dingus 1995). The Large Area Telescope (LAT) aboard the *Fermi* satellite has now recorded photons with energy in the burst rest frame up to 94 GeV, 71 GeV, and 59 GeV from GRB 090902B (de Palma et al. 2009; Cucchiara et al. 2009), GRB 080916C (Abdo et al. 2009a), and GRB 090510 (Abdo et al. 2009b), respectively, demonstrating that the processes in GRBs reach these energies at least. These results highlight the important role for ground-based observatories, sensitive to energies around 100 GeV and above, to seek still higher energy emission or any evidence for a cutoff in the emission mechanism.

Marginal evidence of VHE emission has been reported from the Milagrito air-shower detector (Atkins et al. 2000) and the HEGRA AIROBICC array (Padilla et al. 1998), for two particular bursts, though no conclusive detections have been made. Recent searches with the Milagro (Atkins et al. 2005;

[8] Current address: Disney Interactive Media Group, North Hollywood, CA 91601, USA.
[9] Current address: GEMINI Observatory, Hilo, HI 96720, USA.
[10] Current address: The Claremont Colleges, Joint Sciences Department, Claremont, CA 91711, USA.
[11] Current address: Kent State University, Ashtabula, OH 44004, USA.
[12] Current address: Laboratoire Leprince-Ringuet, École Polytechnique, CNRS/IN2P3, Palaiseau, France.
[13] Current address: McGill University, Medical Physics Unit, Montreal, QC H3G 1A4, Canada.
[14] Current address: Physics and Astronomy Department, University of British Columbia, Vancouver, BC V6T 1Z1, Canada.
[15] Current address: Sander Geophysics Limited, Ottawa, ON K1V 1C1, Canada.

Abdo et al. 2007), Whipple 10 m (Horan et al. 2007), MAGIC (Albert et al. 2007), and H.E.S.S. (Aharonian et al. 2009a) instruments have all reported upper limits.

One of the difficulties faced by atmospheric Cherenkov telescopes (ACTs) and air-shower detectors is that emission above 100 GeV by a GRB is likely to be strongly attenuated on its way to Earth by interacting with the extragalactic background light (EBL) to form electron–positron pairs. The degree of attenuation depends on the redshift of the burst and the density of the EBL at optical/infrared wavelengths. The EBL model of Gilmore et al. (2009), which is consistent with constraints placed on the EBL by recent VHE observations (e.g., Aharonian et al. 2006; Albert et al. 2008), predicts that for a source at a redshift of $z = 0.25$, only ∼7% of the TeV photons emitted would reach the Earth, whereas ∼80% of the 200 GeV photons would be transmitted. For a source at $z = 1$, less than 15% of the 200 GeV flux would be transmitted. For bursts in this study where the redshift is known, this extinction is incorporated into the calculated flux limits.

Another difficulty faced by any telescope with a small field of view is that GRBs are transient events that may fade below the detection threshold of the instrument if the burst cannot be targeted quickly enough.[16] The magnitude of this problem was diminished substantially by the launch of the *Swift* GRB Explorer in 2004. *Swift* is able to localize bursts with a precision of a few arcminutes within ∼20 s of detecting them (Gehrels et al. 2004). *Swift* has performed fast X-ray follow-ups of hundreds of bursts and discovered that about one-third of long GRBs exhibit detectable flares in their X-ray afterglows (Falcone et al. 2007). These flares provide another possible mechanism for creating VHE emission. In addition to SSC emission that might accompany the flare photons, there could be inverse-Compton (IC) emission produced as the flare photons cross the forward shock that produces the underlying afterglow (Wang et al. 2006; Fan et al. 2008).

At the time of *Swift*'s launch, the Solar Tower Atmospheric Cherenkov Effect Experiment (STACEE) was fully operational and capable of beginning GRB follow-up observations within ∼3 minutes of receiving burst coordinates. STACEE was an ACT with an energy threshold of ∼150 GeV for sources at high elevations. After the detector was completed in early 2002, the STACEE Collaboration carried out observations of 23 GRBs, 13 of which were discovered by *Swift*. In this paper, we present these observations and place limits on the VHE flux from these bursts. Although the total number of bursts with published VHE limits is now well over 100, the number probed by ACTs sensitive in the 100–500 GeV energy range within the first 10 minutes after the start of the burst is only 11 or 12 (depending on whether GRB 060602B is included or not), including the three reported here.

2. THE STACEE DETECTOR

STACEE was built at an existing solar-research facility, the National Solar Thermal Test Facility (NSTTF). The NSTTF is located at Sandia National Laboratories in Albuquerque, NM (35.°0 North, 106.°5 West, and 1705 m above sea level). The NSTTF is home to ∼220 large (6.1 m × 6.1 m) heliostats that were designed to focus sunlight on a receiving tower at the south end of the heliostat field. STACEE used 64 of the heliostats, spread over an area approximately 200 m × 150 m, to collect Cherenkov light from extensive air showers. The Cherenkov pulses were reflected to secondary mirrors mounted on the receiving tower. The secondary mirrors were concave spherical mirrors that focused the light onto photomultiplier tubes (PMTs). The geometry results in a field of view about 0.°6 in diameter. There were 64 PMTs, each positioned to receive light from a single heliostat. The STACEE detector is described more completely in Hanna et al. (2002) and Gingrich et al. (2005).

The PMT signals were amplified, split, and sent to flash analog-digital converters (FADCs) and discriminators. Under good observing conditions, the discriminators were set to fire with a pileup of ∼5 photoelectrons. For the purpose of the trigger, the 64 heliostats were grouped into eight clusters of eight heliostats. A level-one (L1) trigger occurred when five out of eight channels in a cluster surpassed their discriminator thresholds within a 24 ns window. A level-two (L2) trigger occurred when five out of eight clusters had L1 triggers in the same 16 ns clock cycle. When an L2 trigger occurred, the event was recorded, including 192 ns samples of the PMT signals from the FADCs.

Due to the sensitivity of the PMTs, STACEE was only operated in dark conditions when the moon was down and there were few clouds in the sky. Under normal operating conditions, the detector was triggered by cosmic-ray showers at a rate of ∼5 Hz. In order to get a precise estimate of the cosmic-ray background, each on-source observation was preceded or followed by an off-source observation at the same azimuth and elevation as the on-source observation. Gamma-ray showers are reconstructed with an angular resolution of 0.°15 (radius, 68% containment) and an energy resolution of 20%.

Between Fall 2004 and Spring 2007, the STACEE collaboration carried out ∼27 hr of observations of the Crab Nebula. After event selection, the on-source event excess was 8.0 times the standard deviation expected from random fluctuations of the cosmic-ray rate (8.0σ). STACEE could detect the Crab at the 5σ level with approximately 10.5 hr on source. A gamma-ray flux that is 4.5 times as strong as the flux from the Crab would have been detected in ∼30 minutes on average.

3. DATA ANALYSIS

The first step in STACEE data analysis is to generate a set of data-quality selection cuts to flag sections of the data that should not be included in the analysis. The primary reasons for cutting data are unstable weather conditions and detector malfunctions. The L1-trigger rates are useful quantities for data-quality cuts because they are very sensitive to the brightness of the night sky, especially in the field of view of the heliostats. If the L1 rates are very erratic during part of a run, that section of the run and the corresponding section of the paired run are flagged to be ignored in the analysis. Similarly, if the behavior of the L1 rates during part of a run is markedly different from the behavior of the L1 rates during the corresponding part of the paired run, those sections are flagged. Data-quality cuts are also made based on the pointing errors of the heliostats and based on malfunctions of the data-acquisition computers.

The rate of cosmic-ray background events that trigger STACEE depends on several factors, such as the detector heading, the transparency of the atmosphere, and the brightness of the field of view. The brightness of the field of view affects the cosmic-ray rate because noise can promote events that would

[16] Gamma-ray burst candidate 060602B occurred serendipitously in the field of view of H.E.S.S. observations of another target (Aharonian et al. 2009b), but it is likely associated with a Galactic X-ray burster rather than a cosmological GRB.

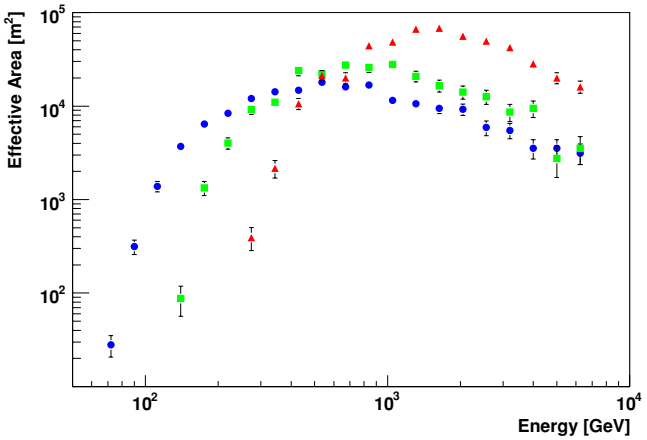

Figure 1. Effective area of STACEE for a source at 84° elevation just south of zenith (blue circles), a source at 59° elevation in the southwest portion of the sky (green squares), and a source at 54° elevation in the northeast portion of the sky (red triangles).

(A color version of this figure is available in the online journal.)

normally be below the trigger threshold and demote events that would normally be above the threshold. Because the energy spectrum of the cosmic rays is a power law that decreases steeply with increasing particle energy, there are many more low-energy showers to be promoted than high-energy showers to be demoted. Thus, the brighter the field of view, the higher the background rate. To correct for this, we employ a technique known as *padding* (Cawley 1994). Padding is the addition of artificial noise in order to balance the noise levels of the PMT signals in the on-source and off-source runs. Once the noise levels are balanced, the trigger criteria are reapplied in software at an increased threshold in order to remove the excess promoted events.

The final event selection that was applied in the analysis of STACEE GRB observations is known as the *grid-ratio cut*. The grid ratio is essentially a measure of how much the profile of an air shower deviates from the shape of a thin, spherical shell. Selecting only events with low grid ratios for analysis enhances the sensitivity of the detector by removing the large majority of the hadronic showers while keeping most of the gamma-ray showers. However, the grid ratio is energy dependent and, therefore, the optimal cut value for a set of observations depends on factors such as the source elevation and discriminator thresholds. For each burst, simulations were used to estimate the optimal cut value that retained at least 60% of the simulated gamma rays; typically about 92% of cosmic-ray showers are rejected. The grid-ratio cut is discussed in detail in Lindner et al. (2007). The event excess detected in observations of the Crab Nebula from 2004 to 2007 was 4.1σ before application of the grid-ratio cut and 8.0σ after the cut.

In order to convert an excess-event rate (limit) into a flux (limit), simulations were used to estimate the effective area of the detector. Air-shower simulations were generated with the CORSIKA package, version 6.203 (Heck et al. 1998). The lists of photons generated by CORSIKA for each shower are fed into a simulation of the STACEE optics (Oser 2000), which generates a list of photoelectrons produced in each PMT. Finally, a detailed electronics simulation applies trigger criteria and generates output files in the same format that is used for real STACEE observations. Gamma-ray showers were simulated at one or more sky positions that were representative of the observations of each burst. Showers were generated with energies between 30 GeV and 10 TeV to determine the effective area of the detector as a function of energy for each observation. Figure 1 shows the effective area after event selection as determined from simulations of three different burst positions.

For a gamma-ray flux dN/dE, the excess-event rate, R, is

$$R = \int_0^\infty \frac{dN}{dE} \times A(E)\, dE, \tag{1}$$

where $A(E)$ is the effective area of the detector as a function of energy. The differential photon-energy spectrum of each GRB was assumed to have the functional form of an intrinsic power law, absorbed by collisions of gamma rays with the EBL, if the redshift is known:

$$dN/dE = C \left(\frac{E}{\mathrm{GeV}}\right)^{-\alpha} \times e^{-\tau_z(E)}. \tag{2}$$

Here $\tau_z(E)$ is the optical depth at redshift z for absorption by the EBL. We used $\tau_z(E)$ from Gilmore et al. (2009); other recent models, e.g., Franceschini et al. (2008) and Finke et al. (2010) are similar. For bursts without a measured redshift, no extinction was assumed, i.e., $\tau_z(E) \equiv 0$. For each burst, limits on the normalization constant, C, were calculated for an assumed spectral index of $\alpha = 2.5$. In addition, limits on the unabsorbed energy flux F between STACEE's energy threshold, E_{th}, and 10 TeV were calculated for each burst, i.e.,

$$F = \int_{E_{\mathrm{th}}}^{10\ \mathrm{TeV}} E \times C \left(\frac{E}{\mathrm{GeV}}\right)^{-\alpha} dE. \tag{3}$$

We define the energy threshold of STACEE as the energy at which the detector response curve ($dN/dE \times A(E)$) reaches its peak; it is given in Table 1 for each burst. Because the optical depth $\tau_z(E)$ increases with energy, when EBL absorption is taken into account, the peak of the detector response curve, hence the threshold, shifts to lower energy. Table 2 shows this effect for GRB 050607, for which the redshift is not known. As the assumed redshift, and therefore amount of EBL absorption, increases the threshold decreases as well as the overall sensitivity. As the fraction of higher energy photons decreases, the low-energy response of the detector, even if small, plays an increased role in the final response to the spectrum.

GRB light curves exhibit extreme variability on timescales that range from fractions of a second to minutes. A brief spike of VHE emission may be washed out in a simple on-minus-off analysis of the entire STACEE data set for a given burst. To search for variability on short timescales, the event rate was calculated in 25-event samples for each on-source run and its off-source partner. For each off-source run, the event rate as a function of time was fitted to a linear function. Each rate measurement in the on-source run was then compared to the value of the off-source fit at the corresponding time in the off-source run.

An alternative method of searching for brief spikes of events in the on-source data is to fit the on-source event rate versus time to a linear function and to search for significant deviations from the fit. This method is not sensitive to slow variations, but it has the advantage that no off-source observation is needed. For two of the GRBs observed with STACEE (GRB 031220 and GRB 061222A), the observing conditions during the off-source runs were dramatically different from the conditions during the on-source runs, so an on-minus-off analysis is not possible. An

Table 1
Summary of STACEE GRB Analysis Results for Assumed Source Differential Photon-energy Spectra of the Form $dN/dE \sim E^{-2.5}$

Burst ID	Energy Thresh. (GeV)	Grid Ratio Cut	Signif.	Flux Upper Limit (99% CL)	
				Photon Normalization, C (m^{-2} s^{-1} GeV^{-1})	Energy Flux, F (erg cm^{-2} s^{-1})
021112	520	0.4	1.44	3.1×10^{-2}	3.4×10^{-10}
030324	540	0.45	0.62	3.0×10^{-2}	3.2×10^{-10}
030501	350	0.425	0.03	3.7×10^{-2}	5.2×10^{-10}
040422	480	0.425	0.61	2.5×10^{-2}	2.9×10^{-10}
040916	330	0.425	0.04	1.2×10^{-2}	1.7×10^{-10}
041016	320	0.425	−1.10	1.8×10^{-2}	2.6×10^{-10}
050209	280	0.4	0.55	2.3×10^{-2}	3.7×10^{-10}
050402	480	0.45	−0.13	3.0×10^{-2}	3.4×10^{-10}
050408	280*	0.45	−0.75	1.0×10^{2} *	1.6×10^{-6} *
050412	240	0.425	1.12	4.7×10^{-2}	8.2×10^{-10}
050509A	530	0.425	−0.01	2.5×10^{-2}	2.7×10^{-10}
050509B	140*	0.375	0.83	2.1×10^{-2} *	5.1×10^{-10} *
050607	160	0.375	−0.98	8.1×10^{-3}	1.8×10^{-10}
060121	650	0.425	−1.93	1.2×10^{-2}	1.1×10^{-10}
060206	110*	0.375	−0.14	1.2×10^{2} *	3.2×10^{-6} *
060323	240	0.4	0.29	1.5×10^{-2}	2.6×10^{-10}
060526	160*	0.425	−0.08	1.1×10^{2} *	2.5×10^{-6} *
061028	520	0.425	0.24	1.1×10^{-2}	1.2×10^{-10}
070223	220	0.425	0.88	1.7×10^{-2}	3.1×10^{-10}
070419A	1800*	0.55	−0.71	9.4×10^{6} *	4.1×10^{-2} *
070610	220	0.4	−2.25	4.5×10^{-3}	8.3×10^{-11}

Notes. These are limits on the average flux for the duration of the STACEE observation of each burst. The photon normalization is the quantity C in Equation (2). The energy flux is the quantity F defined in Equation (3). Entries marked with an asterisk include the effects of EBL absorption, as described in the text, for the redshift given in Table 4.

Table 2
The Effect of EBL Absorption on the STACEE Results for GRB 050607, for which the Redshift is Unknown

Assumed Redshift	0	0.25	0.5	0.75	1	1.3	1.6	2	2.5
Energy threshold (GeV)	160	145	135	130	120	115	110	105	100
Attenuation factor	1	1.7	2.7	4.4	7.1	13	23	48	110

Notes. The attenuation factor is averaged over the STACEE response and the assumed intrinsic power-law spectrum. It is the factor by which the result in Table 1 should be multiplied to obtain the EBL-corrected limit for the corresponding redshift.

additional advantage of this method is that the padding cut, which increases the energy threshold of the analysis, is not necessary (a mild threshold increase was still applied to remove accidental triggers caused by random noise). As before, we measured the event rate in 25-event samples.

4. GRB OBSERVATIONS

4.1. Observing Strategy

GRB observations were one of the top priorities of STACEE. Observers were prepared to retarget the detector at a moment's notice when a new burst was discovered. To facilitate quick responses to GRB discoveries, we developed a GRB rapid alert system. STACEE received alerts from the GRB Coordinates Network (GCN) via internet-socket packets, e-mails, text messages, and pager messages. By having multiple, redundant channels of communication with the GCN, we ensured that every alert was received with minimal delay, even if the network connection at the STACEE site was down or if the observers were not physically at their observing stations.

Both the socket alerts and the e-mail alerts were received and analyzed by alert discrimination software. If an alert appeared to be from a valid GRB detection, a Web page was updated with the burst coordinates and audio alerts were initiated on computers in the heliostat and data-acquisition control rooms. As soon as a burst was localized, the observers on shift immediately terminated any observations that were in progress in order to retarget the detector. The STACEE heliostats could retarget from zenith to an elevation of 45° in ∼1 minute.

Like most STACEE observations, GRB observations were made in pairs of on-source and off-source runs, each typically 28 minutes in length. For GRBs that were less than a few hours old when they became observable, the on-source observation was made first in order to observe the burst at the earliest stage possible. For older bursts, the off-source run was taken first if that would result in observations at higher elevation, and thereby lower energy threshold.

4.2. GRB Observation Overview

The STACEE collaboration carried out follow-up observations of 23 bursts between 2002 June and 2007 July. The bursts were discovered by the *International Gamma-Ray Astrophysics Laboratory* (*INTEGRAL*), *HETE*-2, and *Swift* satellite observatories. Table 3 summarizes the bursts observed by STACEE. Redshift measurements were made for five of the bursts observed by STACEE (Table 4).

The times between the burst triggers and the start of STACEE observations ranged from approximately 3 minutes to 14 hr. There were five cases in which observers received an alert for a burst that was immediately observable. In all other cases, observations began when the sky was dark and the

Table 3
Basic Information about the GRBs Observed with STACEE

Burst ID	Detected By	GRB Time	Duration (s)	Right Ascension	Decl.	Fluence (erg cm^{-2})
021112	*HETE*	03:28:15.89	6.4	39.°27	48.°86	2.1×10^{-7}
030324	*HETE*	03:12:42.80	45	204.°34	−0.°34	1.3×10^{-6}
030501	*INTEGRAL*	03:10:18.49	75	286.°42	6.°31	3.5×10^{-6}
031220	*HETE*	03:29:56.74	16.9	69.°95	7.°38	5.6×10^{-7}
040422	*INTEGRAL*	06:58:05.07	4	280.°55	2.°00	3.4×10^{-7}
040916	*HETE*	00:03:29.70	51.2	345.°44	−5.°56	7.8×10^{-7}
041016	*HETE*	04:39:38.54	33.3	26.°24	−4.°38	4.7×10^{-6}
050209	*HETE*	01:31:41.49	40	126.°61	19.°67	3.0×10^{-6}
050402	*Swift*	06:09:54.58	...	135.°52	16.°57	...
050408	*HETE*	16:22:50.93	14.6	180.°63	10.°84	3.3×10^{-6}
050412	*Swift*	05:44:02.89	26	181.°19	−1.°28	2.1×10^{-6}
050509A	*Swift*	01:46:28.51	11.6	310.°63	54.°09	4.6×10^{-7}
050509B	*Swift*	04:00:19.23	0.03	189.°12	29.°97	2.3×10^{-8}
050607	*Swift*	09:11:22.80	265	300.°23	9.°15	8.9×10^{-7}
060121	*HETE*	22:24:54.50	3.6	137.°62	45.°69	4.9×10^{-6}
060206	*Swift*	04:46:53.27	7	203.°02	35.°04	8.4×10^{-7}
060323	*Swift*	14:32:36.03	213	174.°49	49.°94	5.7×10^{-6}
060526	*Swift*	16:28:29.95	270	232.°91	0.°26	1.1×10^{-6}
061028	*Swift*	01:26:22.46	106	97.°34	46.°27	9.7×10^{-7}
061222A	*Swift*	03:28:52.11	72	358.°33	46.°57	8.3×10^{-6}
070223	*Swift*	01:15:00.68	89	153.°56	43.°09	1.7×10^{-6}
070419A	*Swift*	09:59:26.09	116	182.°81	39.°87	5.6×10^{-7}
070610	*Swift*	20:52:26.14	4.6	298.°87	26.°23	2.4×10^{-7}

Notes. For each burst, the table shows the burst designation, the satellite that discovered the burst, the UT time at which the burst triggered the satellite, the T_{90} duration of the burst, the right ascension and declination of the burst, and the fluence of the burst in the energy range of the satellite detector. For *HETE* bursts, the fluence in the 30–400 keV range is given. For *INTEGRAL* bursts, the fluence in the 20–200 keV range is given. For *Swift* bursts, the fluence in the 15–350 keV range is given. No duration or fluence was reported for GRB 050402 because of the tentative nature of the detection.

Table 4
The Bursts Observed by STACEE that have Measured Redshifts and the Redshift Values

Burst ID	Redshift	Reference
050408	1.236	Berger et al. (2005)
050509B	0.225	Gehrels et al. (2005)
060206	4.045	Fynbo et al. (2006)
060526	3.21	Berger & Gladders (2006)
070419A	0.97	Cenko et al. (2007)

burst coordinates were in a portion of the sky observable with STACEE. For bursts less than ∼2 hr, old observations were carried out at elevations between 30° and 90°. Otherwise, a (nominal) lower elevation limit of 45° was used. Basic information about the follow-up observations carried out with STACEE is shown in Table 5. The rest of this section is devoted to giving more detailed descriptions of the interesting bursts, questionable bursts, and unusual STACEE data.

4.3. GRB 050402

GRB 050402 was detected weakly in a single energy band, eliciting doubts about whether this event was truly a GRB or merely a background fluctuation, and it does not appear in the first *Swift* BAT catalog (Sakamoto et al. 2008). However, the possibility that this event was a soft, weak GRB cannot be ruled out (Barthelmy et al. 2005b), so our observations were treated the same as any other STACEE GRB observation.

Table 5
Summary of Quality-selected Data from STACEE GRB Observations

Burst ID	Time to Target (minutes)	Livetime (minutes)	Initial Elevation
021112	232.7	80	73°
030324	123.9	31	31°
030501	369.8	11	47°
040422	95.3	28	35°
040916	309.7	28	46°
041016	142.0	4.4	51°
050209	217.5	24	56°
050402	4.0	18	49°
050408	642.5	17	43°
050412	7.2	6.9	54°
050509A	476.4	16	53°
050509B	24.2	35	83°
050607	3.2	22	64°
060121	384.7	30	51°
060206	269.8	52	60°
060323	880.5	18	68°
060526	685.6	40	42°
061028	339.2	57	42°
070223	357.9	42	82°
070419A	3.3	27	37°
070610	654.7	24	57°

Notes. The times to target and the livetimes take into account time removed by data-quality cuts. Because of very unsteady observing conditions, none of the data for GRB 031220 or GRB 061222A survived the data-quality cuts.

4.4. GRB 050412

STACEE observations of GRB 050412 began less than six minutes after the burst was detected by *Swift*. Due to an operator error, the first on-source observation was followed by another on-source observation rather than an off-source observation. A third on-source observation was underway when the mistake was noted. The third run was aborted and an off-source run was taken, with a right ascension chosen so that the strip of azimuth and elevation observed matched those of the first on-source observation (a 74 minute offset rather than our standard 30 minute offset). Atmospheric conditions were reasonably stable throughout the observations so we expect the off-source rate to be a reasonable estimate of the background rate of the on-source run, despite the relatively large delay between the observations. However, the imperfect matching in time and elevation between the on and off runs leaves roughly the first minute of data without a reliable background estimate. The usable portion of the run begins seven minutes and 11 s after the burst, as reflected in Table 5.

4.5. GRB 050509B

GRB 050509B is the only short, hard burst observed with STACEE. Due to clouds earlier in the evening, the operators on shift were not ready to begin observations immediately, but were able to get on target approximately 20 minutes after the burst. After data-quality time cuts approximately 35 minutes of livetime remained, with the first uncut observations starting 24 minutes and 12 s after the burst. At the start of observations with STACEE, the burst was at an elevation of approximately 83° and approaching its transit. In terms of the energy threshold of STACEE, the position of this burst in the sky was nearly optimal.

The *Swift* XRT detected a very weak X-ray afterglow in the first few minutes following the burst. This was the first short GRB for which an afterglow was detected (Gehrels et al. 2005). There were also early reports of a variable optical source in the XRT error circle (Cenko et al. 2005a), but it was later determined that the proposed optical counterpart was a steady, extended source (Cenko et al. 2005b). However, within the XRT error circle was a bright elliptical galaxy at a redshift of 0.225 that is widely believed to be the host galaxy for the GRB (Gehrels et al. 2005). The case for this association has been strengthened by the subsequent discovery that other short bursts are associated with nearby, old elliptical galaxies (Barthelmy et al. 2005a). We use the redshift of the galaxy to correct the results for EBL absorption.

4.6. GRB 050607

STACEE began observations of the afterglow of GRB 050607 only 191 s after the burst triggered *Swift*. This is the fastest STACEE GRB follow-up. At the start of observations with STACEE, the burst was at an elevation of approximately 62° in the southern portion of the sky and was rising. The quick response to the burst alert allowed us to observe the burst during a large X-ray flare that occurred 300–500 s after the initial burst. A faint (22.65 mag) optical afterglow was detected with the 4 m Mayall Telescope at Kitt Peak (Rhoads 2005a). The afterglow was particularly faint at blue wavelengths, but whether this was due to a Lyman break or an intrinsically red spectrum is not clear. Based on the observed optical afterglow, a limit of $z < 5$ was placed on the redshift of the burst (Rhoads 2005b).

4.7. GRB 061222A

The *Swift* light curve for GRB 061222A exhibited three main peaks of successively greater intensity. The largest peak occurred 88 s after the *Swift* trigger and had a photon flux of 9.2 cm^{-2} s^{-1} in the 15–150 keV band. The total fluence of the burst in the 15–150 keV band was 8.3×10^{-6} erg cm^{-2} (Tueller et al. 2006), the largest of any of the bursts followed up with STACEE. The burst was also detected by the Konus experiment aboard the Wind satellite. The Konus spectrum between 20 keV and 2 MeV is well fitted by a broken power law with low-energy photon index $\alpha = -0.94$, high-energy photon index $\beta = -2.41$, and peak energy $E_p = 283$ keV (Golenetskii et al. 2006).

The STACEE detector reached the burst coordinates within 4 minutes of the *Swift* burst trigger. Unfortunately, frost began to form on the heliostats during observations of this burst. The main consequences of frost were reduced throughput of photons from the direction of the target and increased background light. As the frost coverage increased, the effects became more pronounced. Therefore, our standard on-minus-off analysis was unsuitable for this data set. Instead, a search for brief spikes on the on-source event rate was performed.

4.8. GRB 070610

Follow-up observations of GRB 070610 detected both X-ray emission (Pagani & Kennea 2007) and optical emission (Stefanescu et al. 2007) from the direction of the burst. However, this counterpart did not exhibit typical GRB-afterglow behavior. The counterpart showed repeated flaring with no overall fading, rather than a decaying light curve. It is believed that this source was a galactic transient rather than a GRB afterglow. The *Swift* trigger was likely caused by a large, high-energy flare of this transient (Pagani et al. 2007) and this event does not appear in Sakamoto et al. (2008), although the possibility that the trigger was caused by a burst with coinciding coordinates cannot be ruled out.

5. RESULTS

Once all cuts were applied, the statistical significance of the on-source event excess for each observation was calculated using the method of Li & Ma (1983). No significant gamma-ray excesses were detected in any of the burst observations. Table 1 shows the statistical significance for each burst along with the upper limits (99% confidence level; CL) on the VHE flux that were calculated using the bounded upper limit method as presented by the Particle Data Group (Barnett et al. 1996). The energy thresholds that were determined from simulations are also shown in the table.

Figure 2 shows the distribution of the on-source rate measurements with respect to the expected event rates (estimated from linear fits of the off-source rates versus time) for all bursts that could be analyzed with on-minus-off analysis. The distribution of off-source rate measurements with respect to the on-source rate fits is also shown for comparison. There were no statistically significant spikes in the rate (in a single bin or across multiple bins).

Figure 3 shows the distribution of the on-source rate measurements with respect to linear fits of the on-source rates versus time for all bursts, including GRB 031220 and GRB 061222A. The distribution of off-source rate measurements with respect to the off-source linear fits is also shown for comparison. When calculating the rates for this plot, the padding cut was not necessary because the on-source and off-source rates were not being

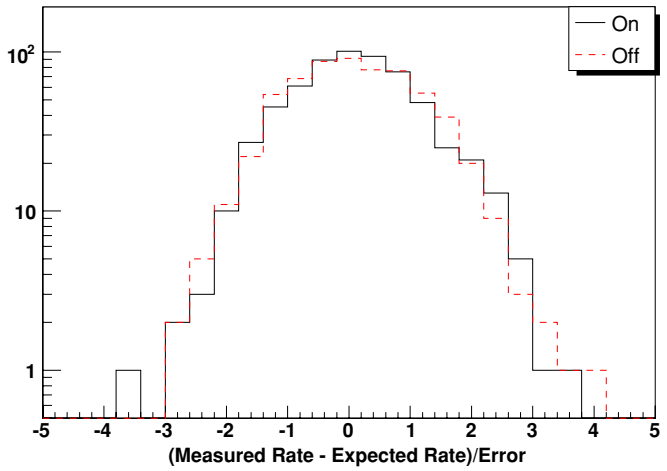

Figure 2. Distribution of measured on-source rates (solid black line), with respect to the rates expected from linear fits of the off-source rates vs. time. This histogram includes all bursts that could reasonably be analyzed with on-minus-off analysis. The event rates (after event selection) vary significantly from run to run, so the difference between the measured rate and the expected rate is expressed in units of the uncertainty in the expected rate ($\sqrt{\text{expected\_events}}$/livetime) in order to combine the results. The distribution of off-source measurements (dashed red line) with respect to the on-source fits is also shown for comparison. In the ideal case of very long observations during which the dependence of the rate on time is exactly linear, we expect these distributions to have width of unity. The standard deviations of the on-minus-off and off-minus-on distributions are 1.04 and 1.07, respectively. There is a slight skew in the distribution shapes due to the fact that only 25 events were used in each measurement.

(A color version of this figure is available in the online journal.)

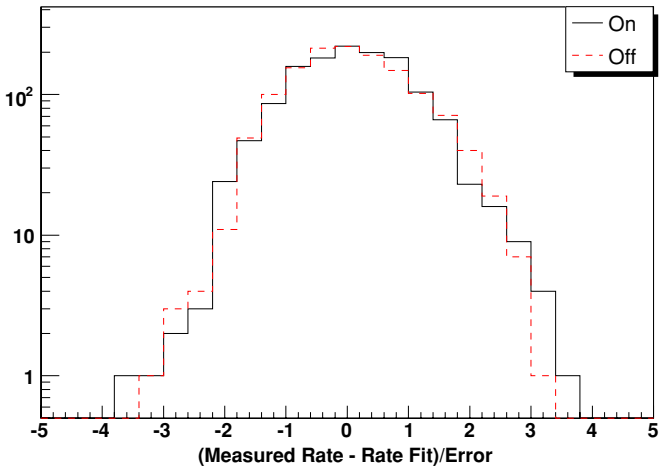

Figure 3. Distribution of measured on-source rates (solid black line), with respect to the rates expected from linear fits of the on-source rates vs. time. This histogram includes all bursts observed with STACEE. The event rates (after event selection) vary significantly from run to run, so the difference between the measured rate and the expected rate is expressed in units of the uncertainty in the expected rate ($\sqrt{\text{expected\_events}}$/livetime) in order to combine the results. The distribution of off-source measurements (dashed red line) with respect to the off-source fits is also shown for comparison. Due to the dependence of the fits on the measurements, we expect the widths of the distributions to be slightly less than unity but to approach unity for very long observations. The standard deviations of the on-source and off-source distributions are 0.98 and 0.97, respectively. There is a slight skew in the distribution shapes due to the fact that only 25 events were used in each measurement.

(A color version of this figure is available in the online journal.)

compared to each other. Instead, a milder threshold increase was applied to remove accidental triggers. There were no statistically significant spikes in the rate.

Figure 4 shows STACEE upper limits on the energy flux between 200 GeV and 10 TeV from GRB 050607 overlaid on the X-ray light curve that was measured by *Swift*. The limits were calculated using an assumed differential photon-energy spectrum of the form $dN/dE \sim E^{-\alpha}$ with $\alpha = 2.0$. Simple power-law fits to the X-ray spectrum during the flare and during the shallow decay after the flare yielded photon indexes of $\alpha \approx 2.3$ and $\alpha \approx 1.8$, respectively (although the flare spectrum was actually fitted better as a harder spectrum with a cutoff at a few keV; Pagani et al. 2006). The rate of gamma-like events detected by STACEE was unusually low during the first ∼200 s of on-source observations for this burst. However, the deficit is not statistically significant, the event rate before applying the grid-ratio cut was normal, and there is no evidence of a detector malfunction.

6. DISCUSSION AND CONCLUSIONS

STACEE performed follow-up observations of 23 GRBs between the summer of 2002 and the completion of the experiment in the summer of 2007. STACEE GRB data include three good-quality observations that began less than five minutes after the bursts were detected by *Swift*. In addition, low-energy-threshold observations were obtained 20 minutes after a short burst with an estimated redshift of 0.225.

No significant gamma-ray excesses were found in any of the observations. Two of the observations were marred by poor weather conditions and could not be reliably analyzed with the on-minus-off analysis technique. Examination of the on-source rates did not yield any strong evidence for short, bright peaks of high-energy emission in the early afterglows of any of the bursts, including these two.

Before the launch of *Swift*, the mean redshift measured for long GRBs was $z \sim 1$. The mean redshift measured for long GRBs discovered by *Swift* is $z \sim 2.3$ (Jakobsson 2008). The higher redshifts of *Swift* bursts mean that any VHE emission from these bursts is more strongly attenuated by interaction with the EBL. The density of the EBL is not precisely known, but recent measurements of TeV blazar spectra imply that the EBL density is near the minimum that can reasonably be expected based on source counts (Mazin & Raue 2007; Albert et al. 2008). Recent models of the EBL density indicate that the optical depth at 100 GeV is less than 1 out to a redshift of about 1.3 (Franceschini et al. 2008; Gilmore et al. 2009), so that a substantial portion of bursts should be amenable to constraining observations. For example, at the assumed redshift of 0.225, the impact of EBL absorption on the results for GRB 050509B is small. For the case we consider with a photon spectral index of 2.5, the overall attenuation factor in the expected number of gamma rays detected with STACEE is 1.6 for the model of Gilmore et al. (2009). This factor is taken into account in the limits give in Table 1. At the other extreme, the high STACEE energy threshold for GRB 070419A (because of the low elevation of the observations) together with the moderate 0.97 redshift combine to raise the limits for this burst by a factor 1.8×10^8 compared to the values with no EBL absorption taken into account.

The result for GRB 050509B is noteworthy since it is the only short, hard burst in the sample and its distance is known, allowing the flux limit to be corrected for EBL absorption. Indeed, this is the first limit on the VHE afterglow within an hour of a short, hard burst with a known distance. The STACEE observations coincide with a faint X-ray afterglow having flux

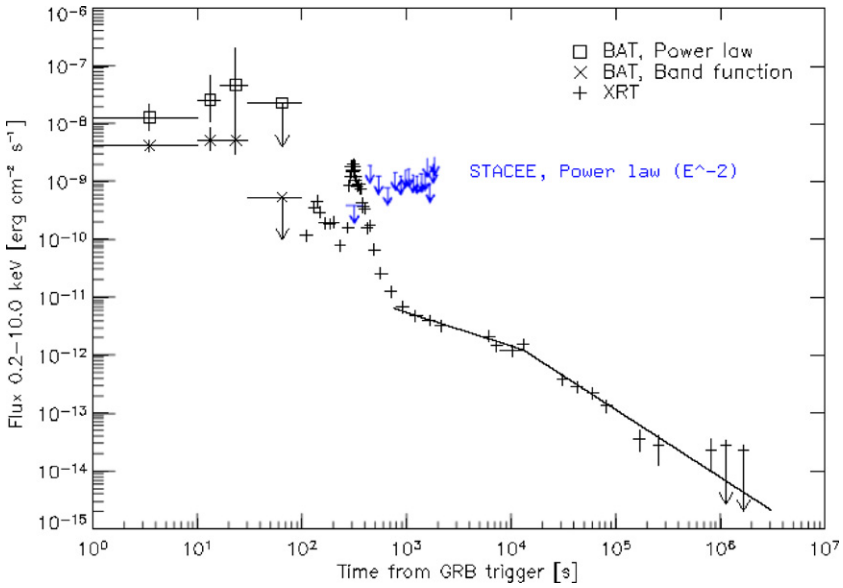

Figure 4. STACEE integral-energy-flux limits superimposed on the afterglow of GRB 050607 measured by *Swift* (from Pagani et al. 2006). The STACEE limits were generated by assuming a source differential photon-energy spectrum of the form $dN/dE \sim E^{-2.0}$, determining an upper limit for the normalization of this spectrum for each point, multiplying the photon-energy spectrum limits by a factor of energy and integrating the result between 200 GeV and 10 TeV. The scale and units for the STACEE limits are the same as those for the *Swift* points.

(A color version of this figure is available in the online journal.)

$\sim$2–7 $\times 10^{-6}$ keV cm^{-2} s^{-1} keV^{-1} at 1 keV (Gehrels et al. 2005). Expressed as νF_ν at 1 keV, the X-ray afterglow is 4–5 orders of magnitude below the STACEE limit on νF_ν at 140 GeV.

The most rapid afterglow measurement with STACEE was obtained for GRB 050607, starting 191 s after the *Swift* trigger and overlapping the detection of an X-ray flare, as shown in Figure 4. The STACEE limit on the flux in Table 1 corresponds to $\nu F_\nu < 1.0 \times 10^{-10}$ erg cm^{-2} s^{-1} at 160 GeV, which is below the value of afterglow predictions in some models, for example in scenarios considered in Pe'er & Waxman (2005) having low circumburst matter density and small contributions from magnetic field to the energy density in the outflow. However, the unknown redshift of this burst makes it difficult to draw firm conclusions from the STACEE results on this burst alone. The effect of EBL absorption on the STACEE response to this burst for several redshifts is summarized in Table 2. The limit is about a factor of 7 weaker if the burst was at redshift 1 and 2 orders of magnitude weaker if the redshift was 2.5. This result may nevertheless prove useful for inclusion in future population studies of the early VHE afterglows from bursts.

In addition to being very distant on average, GRBs have diverse light curves and spectra. Therefore, obtaining an accurate picture of the high-energy behavior of GRBs will ultimately require a large number of fast follow-up observations. The STACEE observations reported here represent a substantial step in that direction. Newer Cherenkov telescopes, such as MAGIC, VERITAS, and H.E.S.S., are now performing GRB follow-up observations with unprecedented sensitivity and with energy thresholds of 100 GeV or lower, although bursts such as GRB 050607 reported here, which are well measured above 100 GeV during the first few minutes after the burst, remain rare. The recent results on high-energy gamma-ray emission from the *Fermi*-LAT, extending to tens of GeV, provide ample motivation for continuing the search at higher energy still.

We are grateful to the staff at the National Solar Thermal Test Facility, who provided enthusiastic and professional support over the years. We thank Scott Barthelmy and the rest of the GCN team for providing an excellent archive of burst information and for helping us create a top-notch GRB-alert system. We thank Rudy Gilmore for providing numerical details of the EBL absorption from his model. This work was supported in part by the US National Science Foundation, NSERC (the Natural Sciences and Engineering Research Council of Canada), FQRNT (Fonds Québécois de la Recherche sur la Nature et les Technologies), the Research Corporation, and the University of California at Los Angeles.

REFERENCES

Abdo, A., et al. 2007, ApJ, 666, 361
Abdo, A., et al. 2009a, Science, 323, 1688
Abdo, A., et al. 2009b, Nature, 462, 331
Aharonian, F., et al. 2006, Nature, 440, 1018
Aharonian, F., et al. 2009a, A&A, 495, 505
Aharonian, F., et al. 2009b, ApJ, 690, 1068
Albert, J., et al. 2007, ApJ, 667, 358
Albert, J., et al. 2008, Science, 320, 1752
Atkins, R., et al. 2000, ApJ, 533, L119
Atkins, R., et al. 2005, ApJ, 630, 996
Barnett, R. M., et al. 1996, Phys. Rev. D, 54, 1
Barthelmy, S. D., et al. 2005a, Nature, 438, 994
Barthelmy, S., et al. 2005b, GCN Circular, 3172
Berger, E., & Gladders, M. 2006, GCN Circular, 5107
Berger, E., Gladders, M., & Oemler, G. 2005, GCN Circular, 3201
Cawley, M. 1994, in Proc. Workshop Towards a Major Cherenkov Detector (Calgary) ed. R. C. Lamb (Ames, IA: Univ. Iowa Press), 176
Cenko, S., et al. 2005a, GCN Circular, 3391
Cenko, S., et al. 2005b, GCN Circular, 3409
Cenko, S., et al. 2007, GCN Circular, 6322
Chiang, J., & Dermer, C. 1999, ApJ, 512, 699
Costa, E., et al. 1997, Nature, 387, 783
Cucchiara, A., et al. 2009, GCN Circular, 9873
de Palma, F., et al. 2009, GCN Circular, 9867
Dingus, B. L. 1995, Ap&SS, 231, 187
Falcone, A. D., et al. 2007, ApJ, 671, 1921
Fan, Y.-Z., et al. 2008, MNRAS, 384, 1483
Finke, J. D., et al. 2010, ApJ, 712, 238
Frail, D. A., et al. 1997, Nature, 389, 261
Franceschini, A., et al. 2008, A&A, 487, 837

Fynbo, J. P. U., et al. 2006, GCN Circular, 4692
Gehrels, N., et al. 2004, ApJ, 611, 1005
Gehrels, N., et al. 2005, Nature, 437, 851
Gilmore, R. C., et al. 2009, MNRAS, 399, 1694
Gingrich, D. M., et al. 2005, IEEE Trans. Nucl. Sci., 52, 2977
Golenetskii, S., et al. 2006, GCN Circular, 5984
Hanna, D. S., et al. 2002, Nucl. Instrum. Methods Phys. Res. A, 491, 126
Heck, D., et al. 1998, Forschungszentrum Karlsruhe Report, FZKA, 6019
Horan, D., et al. 2007, ApJ, 655, 396
Jakobsson, P. 2008, GRB Redshift Sample, http://www.astro.ku.dk/∼pallja/GRBsample.html
Klebesadel, R. W., Strong, I. B., & Olson, R. A. 1973, ApJ, 182, L85
Lindner, T. 2007, APh, 28, L338
Li, T. P., & Ma, Y. Q. 1983, ApJ, 272, 317
Mazin, D., & Raue, M. 2007, A&A, 471, 439
Nemiroff, R. J. 1994, Comments Astrophys., 17, 189
Oser, S. 2000, PhD thesis, Univ. Chicago
Padilla, L., et al. 1998, A&A, 337, 43
Pagani, C., & Kennea, J. A. 2007, GCN Circular, 6490
Pagani, C., et al. 2006, ApJ, 645, 1315
Pagani, C., et al. 2007, GCN Circular, 6520
Pe'er, A., & Waxman, E. 2005, ApJ, 633, 1018
Piran, T. 1999, Phys. Rep., 314, 575
Rhoads, J. 2005a, GCN Circular, 3527
Rhoads, J. 2005b, GCN Circular, 3531
Sakamoto, T., et al. 2008, ApJS, 175, 179
Sari, R., & Piran, T. 1997, MNRAS, 287, 110
Stefanescu, A., et al. 2007, GCN Circular, 6492
Tueller, J., et al. 2006, GCN Circular, 5964
van Paradijs, J., et al. 1997, Nature, 386, 686
Wang, X.-Y., Zhuo, L., & Mészáros, P. 2006, ApJ, 641, L89
Zhang, B., & Mészáros, P. 2001, ApJ, 559, 110